Thermodynamic data for cement clinkering

Theodore Hanein[1, 2, *], Fredrik P. Glasser[3], and Marcus N. Bannerman[2]

[1] *Department of Materials Science & Engineering, University of Sheffield, S1 3JD, United Kingdom*

[2] *School of Engineering, University of Aberdeen, AB24 3UE, United Kingdom*

[3] *Department of Chemistry, University of Aberdeen, AB24 3UE, United Kingdom*

**Corresponding author: theodorehanein@gmail.com*

Abstract

The proportions of cement clinker phases produced by the pyro-processing of a raw-material mix are often predicted through the Bogue equations, established in the 1930s; however, the Bogue approach is limited in its applicability. This presents a challenge as the cement industry is seeking innovative and more environmentally friendly cement clinker formulations and production processes. These often go beyond the limitations of the Bogue equations and more flexible approaches are required. Modern thermodynamic calculations allow this flexibility but rely on databases not freely available and often specialised for other applications. The title paper reviews the thermodynamic data for stoichiometric clinker phases and presents a new dataset. The dataset is validated, and its application demonstrated by case studies. Electronic CSV files containing the data which can be parsed for use with existing Gibbs energy minimisation solvers/software is distributed with this article as supplementary material.

Keywords: Cement; clinker; thermodynamics; dataset; compilation

Cement oxide notation

Oxide	CaO	SiO_2	Al_2O_3	Fe_2O_3	B_2O_3	K_2O	MgO	Na_2O	P_2O_5	SO_3	CO_2	TiO_2
Notation	C	S	A	F	B	K	M	N	P	$	c	T

1 Introduction

Cement is the most manufactured product on earth and its production contributes significantly to greenhouse gas emissions that affect our climate. Carbon dioxide (CO_2) emissions from cement production account for approximately 8% of global manmade CO_2 emissions [1]. These emissions are mainly a result of: (1) raw-material (calcium carbonate calcination) emissions, (2) direct fossil fuel emissions (pyro processing), and (3) electricity-related emissions primarily from grinding. Raw-material emissions alone were estimated to be 1.45 $GtCO_2$ in 2017 [2]. Societal pressures on the cement industry concerning its environmental burden have triggered an increase in the use of alternative fuels and alternative raw materials for cement manufacture [3, 4]. Environmental concerns are also promoting the development of lower-calcium clinker formulations, such as calcium sulfoaluminate cement clinker which contain volatile species and involve gas-solid reactions not normally encountered in Portland cement (PC) clinkering [5].

In conventional cement manufacture, limestone is ground and mixed with specified amounts of other raw materials such as siliceous clays and shales, to achieve a target composition. The raw mix is pyro-processed into clinker in rotary kilns with solid temperatures reaching ≈1500 °C. The indurated product, termed clinker, is cooled rapidly to preserve, insofar as possible, the high temperature phase assemblage, which is thermodynamically unstable at intermediate temperatures but preserved metastably at lower temperatures due to the energy and mixing barriers. The valuable properties of cement arise from this phase assemblage and its interactions with water.

The Bogue equation is often used to estimate clinker phase composition [6]. The calculation assumes that the phase assemblage at the solidus is preserved to ambient, although certain

optional features enable corrections, should equilibrium not be reached during pyro processing, for example failure to assimilate free lime (CaO). Input data for the Bogue calculation are based on the stable coexistence of the four-phase assemblage C_3S-C_2S-C_3A-C_4AF. Variations in temperature, kiln atmosphere, and the presence of minor components, often in the order of several percent by weight total, can influence clinker development but are not included in Bogue calculations and their role is best assessed by thermodynamic calculations.

Bogue-type equations for alternative cements, e.g., calcium sulfoaluminate- based clinkers, have also been developed but have proven unreliable, mainly due to the volatile nature of the sulfur component causing a strong dependence of the stable phases on kiln atmospheres. As process atmospheres are not included in Bogue calculations, the role of complex vapour transport is also not included; however, thermodynamic calculations have enabled theory and experimental data to be reconciled [7-9].

The thermodynamics of cement chemistry have been studied since Le Chatelier [10]; however, much of the literature has focused on hydration where the thermodynamic data are typically valid for temperatures in the range of liquid water. Moreover, calculations often must avoid following equilibrium paths as the occurrence and persistence of metastable phases dominates these reactions. This contrasts with clinkering where a close approach to the high temperature equilibrium is frequently attained.

Thermodynamic tools used for clinker equilibrium calculations include MTData [11] and FactSage [12]. The compiled databases associated with these packages are not freely available but, fortunately, most stoichiometric thermodynamic data of phases related to cement are recorded in the literature. Solid solution models are often used to correlate the

properties of complex solid phases, such as the clinker ferrite phase (C_2(A,F). Melt formation is desirable during clinkerisation to provide a medium/flux for reactive transport/mixing. Therefore, solid and liquid solution models provide the best approach to calculating clinker equilibrium; however, the data required to support calculation of solution models and of solid-liquid-gas equilibria are as yet incomplete and existing models are often parametrized using data derived for other industries (such as metallurgy) and cannot be directly re-purposed for use in cement clinkering.

The utilization in cement kilns of alternative fuels and wastes that can contain or develop volatile species, coupled with the development of alternative binders, present new challenges. For example, the role of the kiln atmosphere in cement production becomes more important; the partial pressure of gases such as CO_2, O_2, and SO_2 can greatly influence mass transfer and reaction progression within the kiln [13-16]. This is particularly true for volatile components such as calcium carbonate (Cc), calcium sulfate (C$), spurrite ($C_5S_2$c), ye'elimite ($C_4A_3$$), ternesite ($C_5S_2$$), and many alkali chlorides, sulfates, and carbonates.

The title study suggests gas phase thermodynamic data that can be used to simulate process atmospheres and reviews, compiles, and presents a thermodynamic database of stoichiometric phases, which can be used for heat balances and limited predictive modelling of clinkering. The database is evaluated and its importance, limitations, and required additional developments are discussed.

2 Survey of thermodynamic data for cement clinkering

2.1 Gas phase thermodynamic data

The National Aeronautics and Space Administration (NASA) developed a thermodynamic data-set (NASA CEA database) [17] of gaseous species and solid phases used in rocket combustion calculations. It is a parameterisation of many historical collections and includes extrapolation as high as 20,000K for many gas species. It forms the foundation of many combustion models (e.g., GRI MECH [18]) and is suited for modelling atmospheric reactions at kiln temperatures. This database also contains necessary solid and liquid thermodynamic data for salts and simple oxides. As this database also contains reference data for elements which have been extensively reviewed over decades, this compilation is used as the reference against which database of the title study is constructed/compared.

2.2 Solid and liquid phase thermodynamic data

Other compilations [19-27] contain thermodynamic data for pure solid and liquid phases; however, most are outdated as new material properties have been recently measured and existing thermodynamic data have been re-evaluated. Babushkin and his co-authors [19] were pioneers in compiling relevant thermodynamic data and their work contains thermodynamic data for the major PC clinker phases. However, transcription [19] introduces errors such as the heat capacity coefficients for C_3A, which differ from those in the original [28]; and have been propagated into other compilations [29]. Indeed, the authors of the title paper believe that the current limited success in applying free-energy minimisation techniques to clinker calculations may have its roots in similar error propagation.

Haas Jr et al. published a thermodynamic data compilation [20] which has proven very useful [30]. Data for many of the species involved in cement clinkering are compiled; however, it contains a number of errors as some of the expressions given do not agree with the sample data (where available) or with reference points; e.g., data for H_2O, AlO(OH), and Si. The readily available portable digital scan of this benchmark compilation [20] also seems to have a missing negative sign in the enthalpy constant (a2) for CAS. There are uncertainties in the data validity regions, for example; the reported valid temperature ranges for C_3AS_3 differ between the provided functions and the calculated tables. The data for polymorphs of C_2S are differentiated in this compilation; however, hatrurite and other polymorphs of C_3S (the major phase in Portland cement) are undifferentiated probably because the data available either at that time (or now) are not known.

A thermodynamic data compilation by Kelley [26] contains data for cement phases not included in Ref. [19]. Most of Kelley's data [26] are taken from experiments carried out by the United States Bureau of Mines; however, numerous misprints occur (e.g. in the data for C_2P) and unnecessary numerical rounding was introduced in equation coefficients which significantly affects the accuracy of any subsequent calculations carried out using their expressions. Data extracted from [26] are best reviewed after checking with the source.

NIST has tabulated reference thermodynamic properties [25] at standard conditions of 298.15 K and 1 bar for numerous species relevant to cement clinkering. This publication also corrects some previous experimental measurements, such as the heats of formation of calcium aluminates [31] by preferring data from Huber and Holley [32] who also re-evaluated the heat of formation of CaO. This tabulation is used as the main source for reference data in the title study, but one notable exception is the standard heat of

formation for CA_2. Contradictory experimental values for the heat of formation of CA_2 are presented [25, 27, 33, 34]. The database presented in the title study was used to reproduce the phase diagram of the C – A binary system [35]and the best fit data of Petaev [34] is selected.

Hillert et al. [36] encountered difficulties when performing equilibrium calculations for the C–S binary system using available literature data and therefore reassessed the data for rankinite; these data [36] are adopted in the title study in preference to those of Haas Jr et al. [20].

More recent data-sets that contain thermodynamic data for species related to cement clinkering were developed by Holland and Powell [21, 37]. These datasets are internally consistent but do not contain data for the major cement clinker phases.

2.3 The calcium alumino-ferrite phase

The calcium alumino-ferrite (C_2(A, F)) composition found in cement clinkers should be modelled thermodynamically as a solid solution as the A/F ratio varies. Moreover, and owing to fractionation during cooling, the ferrite is often compositionally zoned. Babushkin et al. [19] presented thermodynamic data for C_4AF; however, the sources cited for their data is not readily available and could not be checked. The standard enthalpy of formation of C_4AF has been derived by Thorvaldson et al. [38] and Zhu et al. [39] derived its Gibbs energy data over wide temperature range.

A significant typographical error related to the CF phase discovered in the literature is a typo of 10^{-5} instead of 10^5 in Ref. [40] for the heat content of CF (crystal). Apart from the heat of formation of C_6A_2F available in Refs. [41, 42], the authors are unaware of other

stoichiometric thermodynamic data for calcium alumino-ferrites. As this study does not consider solid solution models, assuming that C_4AF is the stable ferrite solid solution under clinker processing conditions allows a single dataset to be used up to the eutectic; 1338 °C[a] for PC clinker [43] and 1275 °C[a] for calcium sulfoaluminate clinker [44].

3 Compiled thermodynamic data set

The thermodynamic data set presented here have slightly different reference pressures (1 bar or 1 atm) but they all have the same reference temperature (298.15 K) and reference state, i.e., the enthalpy of formation of the elements at the standard temperature and pressure is zero for O_2, Si, H_2, Al, Ca, Fe, etc. No corrections are made for the differences between reference pressures; however, all the gas data are at the same reference pressure, 1 atm. In addition, no accommodation is made for changes in the temperature standard or isotopic composition. Reference elemental data used in the source literature have been reviewed but generally no adjustment was needed. Formula weights for unit conversion were estimated using the CIAAW[b] isotopic abundances [45] along with the AME2012 atomic mass evaluation [46, 47].

The thermodynamic model assumes ideal gases and incompressible solid phases. This allows the thermodynamic data to be fit using a heat capacity polynomial,

$$C_{p,\alpha}(T) = \sum_i C_{i,\alpha}\, T^i,$$

[a] These reported temperatures should only be used as guides and the actual clinker melting temperatures will vary depending mainly on iron, alumina, and alkali content of the mix.
[b] Isotopic abundances were taken from the table given by CIAAW. This data was scraped on 29/07/2015. https://www.ciaaw.org/isotopic-abundances.htm

where $C_{p,\alpha}$ is the temperature-dependent heat capacity of a pure component α and $C_{i,\alpha}$ is a fitting constant for the i^{th} power of temperature. Varying powers appear depending on the source data set with as many as nine terms for NASA CEA data. Two additional fitting constants for the entropy, s_α^0, and enthalpy, h_α^0, allow the chemical potential at standard conditions in pure phases, μ_α^0, to be fit as follows,

$$\mu_\alpha^0(T) = C_{-1,\alpha}(\ln T + 1) - C_{0,\alpha}\,T(1 - \ln T) + h_\alpha^0 - T\,s_\alpha^0 + \sum_{i\neq -1,0} \frac{C_{i,\alpha}}{i(i+1)} T^{i+1}.$$

To model pressure and mixing effects in gas phases, the ideal gas approximation is used,

$$\mu_\alpha(T, \{x_\alpha\}^{N_s}) = \mu_\alpha^0(T) + R\,T\,(\ln(p/p_0) + \ln x_\alpha) \qquad \text{(for an ideal gas)},$$

where p is the system pressure, p_0 is the reference pressure at which the heat capacity data was collected, and x_α is the mole fraction of species α. For incompressible phases, such as liquids and solids, the following model is used,

$$\mu_\alpha(T, \{x_\alpha\}^{N_s}) = \mu_\alpha^0(T) + v_\alpha(p - p_0) + R\,T \ln x_\alpha \quad \text{(for an incompressible solid/liquid)},$$

where v_α is the species molar volume which is assumed to be zero for this iteration of the database. In addition, all solid phases are assumed to be pure and liquids/melts and gases are assumed to mix ideally. This is a significant approximation and thus results where melts are predicted should be treated with scepticism.

Table I presents the phases considered in this work whose thermodynamic data have been taken from a single source. The thermodynamic data taken from Haas Jr et al. [20] were compared with the tables of calculated data (also contained within Ref. [20]) and some enthalpy constants have been corrected where necessary (see Table I for details). Table II presents the thermodynamic data taken from Haas Jr et al. [20] but including the

corrections made which go beyond a simple enthalpy correction. Table III presents the thermodynamic data and its source for phases whose data have been compiled and fitted from separate sources for the title study. Table IV presents data for CA_2, CA_6, and A_3S_2 taken from separate single sources, and are not compatible with the format of Table III. Where reference values for species are not provided by Haas Jr et al. [20], they are calculated from the provided tabulated data in [20]. The thermodynamic data taken from the NASA CEA and Holland and Powell databases are not presented in the title paper and are readily available online.

Thorvaldson et al. [38] derived the standard enthalpy of formation of C_4AF and Zhu et al. [39] presented its Gibbs energy over the temperature range 298 – 2000 °C. Coupling this information [39] with the readily available thermodynamic data of the oxides, a new set of thermodynamic data for C_4AF is derived and presented in this work (see Table III). The C_4AF data derived in the title paper is preferred over the data by Babushkin [19]. This is justified by the observation in Ref. [13] where clinker equilibrium calculations using the Babushkin data predict that C_4AF is never stable, which is contradictory to well-known experimental observations [35]; C_4AF is stable using the data in the title study.

Data for some boron-containing phases are provided in Table III; these were initially compiled due to industrial interest in making boron-containing calcium sulfoaluminate cement; however, these values should be used cautiously as no simulations or validations including these phases have been conducted in the course of the title study.

Table I: Species considered in the title study whose thermodynamic data were taken from a single source. Values displayed between vertical bars (|) represent the number of polymorphs available in the database.

Ref.	Phase	Species
[17]	*Liquids*	H_2O, $MgCO_3$, $KAlO_2$, Na_2CO_3, Na_2O, K_2O, Na_2SO_4, K_2CO_3, K_2SO_4, $K_2Si_2O_5$, K_2SiO_3, $MgSiO_3$, $CaSO_4$, $CaCO_3$, B_2O_3
	Solids	$CaCO_3$, Mg_2SiO_4, Fe_2O_3 |2|, $MgCO_3$, $KAlO_2$, Na_2CO_3 |3|, Na_2O |3|, $NaAlO_2$ |2|, K_2O |3|, Na_2SO_4 |3|, K_2CO_3 |2|, K_2SO_4 |2|, MgO, $K_2Si_2O_5$ |3|, K_2SiO_3, $MgSiO_3$ |3|, $CaSO_4$ |2|, $MgTiO_3$, Mg_2TiO_4, $MgTi_2O_5$, Ti_3O_5 |2|, TiO_2 , TiO |3|, Ti_2O_3 |2|, Ti_4O_7, B_2O_3
[20]	*Solids*	$AlO(OH)^a$ |2|, $Al(OH)_3$, $CaAl_2SiO_6$, $CaAl_2Si_2O_8$, $CaAl_2Si_3O_{10}(OH)_2{}^a$ $CaAl_2SiO_7$, $Ca_3Al_2Si_3O_{12}$, $Al_2Si_4O_{10}(OH)_2$, $Al_2Si_2O_5(OH)_4$ |3|, Al_2O_3, Al_2SiO_5 |3|, $Ca_2Al_3Si_3O_{12}{}^a$, $CaAl_4Si_2O_{10}(OH)_2{}^a$, CaO, $CaSiO_3$ |2|, Ca_2SiO_4 |4|, Ca_3SiO_5, SiO_2 |2|
[21]	*Liquids*	$NaAlSi_3O_8$, $CaAl_2Si_2O_8$, $CaMgSi_2O_6$, $Mg_2Si_2O_6$, Fe_2SiO_4, Mg_2SiO_4, $KAlSi_3O_8$, Al_2SiO_5
	Solids	$Ca_5Si_2CO_{11}$, $CaMgC_2O_6$, $Ca_5Si_2C_2O_{13}$, $NaAlSi_3O_8$ |2|, $CaMgSi_2O_6$, $Mg_2Si_2O_6$, $KAlSi_3O_8$, $NaAlSi_2O_6$, Fe_2SiO_4, $Fe_2Si_2O_6$
[34]	*Solids*	$CaAl_{12}O_{19}$, $CaAl_4O_7$
[48]	*Solid*	$Al_6Si_2O_{13}$
[36]	*Solid*	$Ca_3Si_2O_7$

[a] denotes species whose enthalpy constants have been corrected.

Table II: Thermodynamic data (including corrections) adapted from Ref. [20]. T_{min} and T_{mix} show the temperature range over which the data is valid. Units of Cp are in J mol^{-1} K^{-1}. This table is provided in comma-separated values (CSV) format in the supplementary material (S1).

Species	**Polymorph**	$\boldsymbol{h}(298.15\boldsymbol{K})$ **(J/mol)**	$\boldsymbol{T_{min}}$ **(K)**	$\boldsymbol{T_{max}}$ **(K)**	$\boldsymbol{C_{-2,\alpha}}$	$\boldsymbol{h_{\alpha}^{0}}$	$\boldsymbol{C_{-0.5,\alpha}}$	$\boldsymbol{s_{\alpha}^{0}}$	$\boldsymbol{C_{0,\alpha}}$	$\boldsymbol{C_{1,\alpha}} \times 10^{3}$	$\boldsymbol{C_{2,\alpha}} \times 10^{5}$
A	Corundum	-1675711	200	1800	0	17321	-2465.18	-1550.92	233.004	-19.5913	0.94441
0.5×AH	Diaspore	-999456	200	800	243069	15671.57	-1730.02	-1021.486	150.556	0	0
	Boehmite	-990420	200	800	777111	30456.1	-2592.74	-1426.36	206.903	0	0
$0.5\times AH_3$	Gibbsite	-1293334	200	800	661704.4	25824.3	-2667.64	-1513.072	220.8509	30.06455	0
AS	Kyanite	-2594270	200	1800	0	23795.1	-3557.46	-2234.89	336.114	-12.98	0
	Andalusite	-2590270	200	1800	2287510	87578.7	-6754.36	-3712.02	543.227	-103.545	6.68935
	Sillimanite	-2587774	200	1800	0	16676.2	-3164.868	-2050.871	313.4705	-9.47081	0
AS_2H_2	Dickite	-4118475	200	1000	3804450	137944.8	-11195.31	-6190.732	908.3598	-105.6632	0
	Halloysite	-4101028	200	1000	1936712	84151.4	-8729.481	-5153.86	772.3004	-72.58844	0
	Kaolinite	-4119800	200	1000	1491950	73551.4	-8278.64	-4973.66	749.175	-67.7102	0
AS_4H	Pyrophyllite	-5642023	200	1000	6069358	231127	-17742.85	-9850.236	1454.512	-396.0932	39.71889
C	Lime	-635094	200	1800	-255577	-7058	-431.99	-420.068	71.6851	-3.08248	0.223862
CS	Wollastonite	-1634766	200	1800	0	3025.9	-1729.6	-1212.413	192.7733	-9.115107	0.4413189
	Cyclo-wollastonite	-1627614	200	1800	-9739.076	-2474.4	-1372.368	-1024.504	167.2547	-0.3621589	0
C_2S	gamma	-2316534	200	1150	-2360066	-73871.8	1656.378	239.1441	0	106.5862	-8.150119
	alphaprime	-2309710	950	1750	0	-48354.4	0	-805.6381	161.6203	0	1.8897
	alpha	-2317614	1650	1800	0	-59510	0	-1052.325	199.6	0	0
	beta	-2306697	200	1000	0	-2120.9	-2094.286	-1538.485	249.689	0	0
C_3S		-2933130	200	1800	-65259.72	-4046	-2766.085	-2053.31	333.9197	-2.325287	0
CAS	Ca-Al Clinopyroxene	-3298900	298.15	2000	-2720240	-29896.3	-2185.82	-1966.33	322.848	0	0
CAS_2	Anorthite	-4227800	200	1800	3185910	110301	-9449.81	-5358.32	800.971	-146.45	10.5663
C_2AS	Gehlenite	-3981700	200	1800	1510470	51954.3	-6274.33	-3822.22	588.351	-67.1533	3.89086
C_3AS_3	Grossular	-6636300	200	1600	1770800	90229.2	-10707.7	-6532.38	985.362	-96.6435	3.35314
C_2AS_3H	Prehnite	-6193631	298.15	1250	2755226	96995.98	-10560.51	-6270.704	946.022	-57.53272	0
$0.5\times C_4\ A_3S_6H$	Zoisite	-6891117	200	1250	0	34330.83	-8148.754	-5391.475	834.6223	-19.84469	0
CA_2S_2H	Margarite	-6239610	200	1250	0	46846.6	-8427.438	-5406.581	826.504	-25.14555	0
S	alpha	-910699	200	844	0	1058	-777.338	-529.232	83.2101	10.9962	0
	Beta	-911268	844	1800	0	-18010.85	0	-300.994	58.9107	5.0208	0

Table III: The sources and thermodynamic data of species included in the title study. Where a symbol follows the species, this denotes whether the species is a liquid (L) or it denotes the polymorph of the crystal phase (α, β, or γ); where no symbol follows the species, this implies the species is a crystal with no polymorphism. The range in which the data are valid are represented by T_{min} and T_{max}. Units of Cp are in J mol^{-1} K^{-1}. This table is provided in comma-separated values (CSV) format in the supplementary material (S2).

Species	$\boldsymbol{s}(298.15\boldsymbol{K})$ **(J/mol/K)**	**Ref**	$\boldsymbol{h}(298.15\boldsymbol{K})$ **(J/mol)**	**Ref**	$\boldsymbol{C}_{0,\alpha}$	$2\boldsymbol{C}_{1,\alpha} \times 10^{3}$	$-\boldsymbol{C}_{-2,\alpha} \times 10^{-5}$	$\boldsymbol{h}_{\alpha}^{0}$	$\boldsymbol{T}_{min}$ **(K)**	$\boldsymbol{T}_{max}$ **(K)**	$\boldsymbol{s}(\boldsymbol{T}_{min})$ **(J/mol/K)**	**Ref.**
$C_{12}A_7$ α	1046.8	[25]	-19430000	[25]	1263.40064	137.026	231.3752	-466478.34	298	1310		[28]
$C_{12}A_7$ β	1046.8	[25]	-19430000	[25]	956.12768	205.93648	0	-164544.17	1310	1700	2022.5456	[28]
C_2B (L)	145.1	[25]	-2734410	[25]	285.3488	0	0	-70082	1585	1900	410.032	[49]
C_2B α	145.1	[25]	-2734410	[25]	183.05	24.058	44.72696	-71717.94	298	804		[49]
C_2B β	145.1	[25]	-2734410	[25]	218.78136	5.0208	0	-77960.47	804	1585	190.12096	[49]
C_2F	188.78	[25]	-2139280	[25]	247.86016	0	48.86912	-90290.72	298	1750		[40]
C_2F (L)	188.78	[25]	-2139280	[25]	310.4528	0	0	-45940.32	1750	1850	497.51944	[40]
C_3A	205.9	[25]	-3587800	[25]	260.57952	9.58136	50.24984	-95399.38	298	1800		[28]
C_3B	183.7	[25]	-3429080	[25]	236.14496	21.79864	54.47568	-90730.04	298	1760		[49]
C_3B (L)	183.7	[25]	-3429080	[25]	393.296	0	0	-148113.6	1760	1900	538.0624	[49]
C_3S_2	210.37	[36]	-3951761	[36]	251.375	29.491	48.262	-93756	293	2500		[36]
C_4AF	427.28	[39]	-5076016	[38]	374.42616	36.4008	0	-114871.2	298	1863		[19]
CA	114.22	[25]	-2326300	[25]	150.624	12.46832	33.30464	-57186.91	298	1800		[28]
CB	104.85	[25]	-2030960	[25]	129.78768	20.41792	33.76488	-51835.58	298	1435		[49]
CB (L)	104.85	[25]	-2030960	[25]	258.1528	0	0	-117695.92	1435	1700	283.80072	[49]
CB_2	134.7	[25]	-3360250	[25]	214.80656	40.08272	71.79744	-91688.18	298	1260		[49]
CB_2 (L)	134.7	[25]	-3360250	[25]	444.7592	0	0	-198907.36	1260	1800	438.52504	[49]
CF	145.35	[25]	-1520340	[25]	164.93328	9.95792	15.31344	-55203.7	298	1510		[40]
CF (L)	145.35	[25]	-1520340	[25]	229.7016	0	0	-21045.52	1510	1800	355.34712	[40]
CT α	93.64	[25]	-1660600	[25]	127.48648	2.84512	27.99096	-47651.58	298	1530		[50]
CT β	93.64	[25]	-1660600	[25]	134.01352	0	0	-46848.25	1530	1800	202.2964	[50]
CTS	129.2	[25]	-2603300	[25]	177.35976	11.58968	40.29192	-67425.16	298	1670		[51]
CTS (L)	129.2	[25]	-2603300	[25]	279.4912	0	0	-79454.16	1670	1811	389.65592	[51]
FS	145.2	[25]	-1479900	[25]	152.75784	19.58112	28.0328	-56689.02	298	1490		[52]
FS (L)	145.2	[25]	-1479900	[25]	240.58	0	0	-50015.54	1490	1724	339.15504	[52]
FT	105.86	[53]	-1246400	[27]	116.60808	9.12112	20.053912	-42304.42	298	1640		[50]
FT (L)	105.86	[53]	-1246400	[27]	199.1584	0	0	-61262.13	1640	1800	267.65048	[50]
M_2S	95.14	[25]	-2174000.12	[25]	149.82904	13.68168	35.64768	-57843.8	298	1808		[52]

M_2T	109.33	[25]	-2165200	[25]	150.45664	17.86568	28.82776	-56115.81	298	1800		[54]
MA	80.63	[25]	-2299900.03	[25]	153.9712	13.3888	40.91952	-60822.81	298	1800		[28]
MF α	123.8	[25]	-1428400	[25]	88.11504	93.26136	0	-34564.02	298	665		[40]
MF β	123.8	[25]	-1428400	[25]	189.9536	0	0	-61044.56	665	1230	139.36904	[40]
MF γ	123.8	[25]	-1428400	[25]	107.40328	28.40936	0	-1033.45	1230	1800	257.35784	[40]
MT	74.56	[25]	-1572800	[25]	118.36536	6.86176	27.32152	-45065.86	298	1800		[50]
MT_2	127.28	[25]	-2509600	[25]	170.20512	19.2464	30.7524	-62772.55	298	1800		[54]
NT (L)	121.67	[25]	-1591199.89	[25]	196.2296	0	0	-16484.96	1303	1600	290.5788	[55]
NT α	121.67	[25]	-1591199.89	[25]	105.35312	43.34624	0	-35266.94	298	560		[55]
NT β	121.67	[25]	-1591199.89	[25]	108.5748	35.564	0	-32969.92	560	1303	92.08984	[55]

Table IV: Revised thermodynamic data for CA_2, CA_6, and A_3S_2. The temperature range over which the data are valid are represented by T_{min} and T_{max}. Units of Cp are in J mol^{-1} K^{-1}. This table is provided in comma-separated values (CSV) format in the supplementary material (S3)

Species	$\boldsymbol{s}(298.15\boldsymbol{K})$ **(J/mol/K)**	$\boldsymbol{h}(298.15\boldsymbol{K})$ **(J/mol)**	$\boldsymbol{C}_{0,\boldsymbol{\alpha}}$	$\boldsymbol{C}_{-0.5,\boldsymbol{\alpha}}$	$\boldsymbol{C}_{-2,\boldsymbol{\alpha}} \times 10^{-7}$	$\boldsymbol{C}_{-3,\boldsymbol{\alpha}} \times 10^{-9}$	$\boldsymbol{C}_{1,\boldsymbol{\alpha}} \times 10^{2}$	$\boldsymbol{C}_{2,\boldsymbol{\alpha}} \times 10^{5}$	$\boldsymbol{T}_{\boldsymbol{min}}$ **(K)**	$\boldsymbol{T}_{\boldsymbol{max}}$ **(K)**	**Ref**
A_3S_2	254.3872	-6848057	853.677	-9818.19377	0.547237701	0	0.64178016	-1.92257126	298	2000	[48]
CA_2	172	-4007000	310.64	-395.88	-1.4152	1.6974	1.04	0	200	2000	[34]
CA_6	391.7	-10715000	818.02	-579.13	-3.8774	4.3798	1.846	0	200	2000	[34]

Together, these tabulations make up a thermodynamic database for cement clinkering equilibrium calculations.

4 Validation

In order to calculate the clinker products resulting from a particular raw feedstock and processing environment we consider equilibrium where the temperature and pressure are equal among all phases and the entropy is at a maximum using the solver described by Hanein et al. [13]. For fixed pressure and temperature, the Gibbs energy $G = \sum_\alpha N_\alpha \, \mu_\alpha$ is minimised until the difference between iterations is less than 0.001% by mass for each component. The IPOPT package is used to provide the minimisation [56].

4.1 Clinker mineral composition

The thermodynamic data are first validated here against thermodynamic clinkering calculations carried out by Hökfors et al. [57] where the equilibrium calculations were performed at 1360 °C followed by Scheil cooling [c]; the raw meal composition was: 77:36% $CaCO_3$, 13.73% SiO_2, 2.93% Al_2O_3, 1.843% Fe_2O_3, 1.83% MgO, 0.85% K_2O, 0.14% Na_2O, 1.08% SO_3, 0.153% TiO_2, 0.06% Cl, 0.02% P_2O_5, and 0.01% ZnO (by mass). This same raw meal and temperature were used in the title study to calculate equilibrium; but, P_2O_5, ZnO, and Cl were neglected owing to insufficient thermodynamic data. The initial atmospheric composition is air and the input mass of air are assumed to be 1 g per gram of raw meal. The results are compared to those calculated by Hökfors et al. [57] and to the original Bogue calculations, Table V.

[c] Scheil cooling is a constrained equilibrium approach, used in metallurgy for the redistribution of phases in a melt during cooling. The approach assumes that once a component has partitioned from the liquid to the solid phase, it does not undergo further reaction.

Table V: A comparison of clinker equilibrium calculations between results from this work, literature, and Bogue calculations (all in wt. %). (C-A-F) represents the sum of all calcium aluminate ferrite solid solutions reported by Hökfors et al. [57]

Phase	**Equilibrium** [57]	**Scheil cooled** [57]	**Bogue calculations***	**Title study**
C_3S	72.3	72.3	75.2 (80.3)	76
C_2S (stoichiometric)	-	-	2.9 (3.1)	3.4
C_2S (solid solution)	3.5	6.2	-	-
(C-A-F)	0	14.5	-	-
C_3A	-	-	7 (7.5)	7.2
C_4AF	-	-	8.5 (9.1)	8.6
M	2.3	3	-	2.8
CT	-	-	-	0.4
Na_2SO_4 (L)	-	-	-	0.1
K_2SO_4 (L)	-	-	-	1.4
CaO	1.3	2	-	0
Salt melt	0.8	1.3	-	-
Oxide melt	19.7	0	-	-

* Values in parenthesis are normalised to 100%

Direct comparison of the results of the present study with those of Hökfors et al. [57] and the Bogue calculation are complicated by a number of factors. Several versions of Bogue exist differing in assumptions although all are based on phase relations at the solidus temperature. But different assumptions can be made about the course of cooling and its impact on phase development. For example , Hökfors et al. [57] defines two states, 1) a high temperature state "equilibrium" consisting of solid phase(s) and melt, and 2) an assumption about cooling (Scheil cooling) where melt crystallises without reaction with previously formed crystals.

It is known that "melt" invariably crystallises under industrial conditions, giving rise to belite, ferrite and aluminate, etc; these cumulate with crystal totals formed above the solidus. This condition accords most closely with Scheil cooling which allows additional belite to form (see Table V).

What can be concluded is that the Bogue results, derived from experiment, and those of the title study, derived from first principals using thermodynamic data are in accord. The Bogue weight percentage calculations do not initially add up to 100%; this is due to the raw meal containing species which are not accounted for in the general four-phase (C_3S, C_2S, C_3A, C_4AF) Bogue assumption. Although calculations presented here do not take into account solid solutions, the final clinker products can still be deduced assuming that there are no significant phase changes during rapid cooling other than polymorphic transformations which are isochemical. This holds true for pure compounds but in solid solutions exsolution may occur upon cooling. The predicted formation of alkali sulfates is justified as clinkers are well known to contain alkali sulfates [58]. The agreement between the predictions appears to validate the use of a purely stoichiometric thermodynamic approach for traditional clinkering.

The Bogue equations capture the output of the thermodynamic calculations as indeed they should; however, thermodynamic simulations can be taken beyond the limitations of the Bogue equations and examples are given below.

4.2 Phase evolution during clinkering

A Portland cement clinker composition, taken from Ref. [35], is: 67.0% CaO, 22.0% SiO_2, 5.0% Al_2O_3, 3.0% Fe_2O_3, 1.0% MgO, 1.0% K_2O, and 1.0% TiO_2 by mass. Calculations are performed to show the equilibrium evolution of phases during heating and contrast this with observations. The reactions at lower temperature are sensitive to process atmosphere and the composition during clinkering depends on the partial pressures of oxygen and carbon dioxide. For this calculation example, the atmosphere was assumed to have been generated from the

combustion of methane (natural gas) in 15% excess air. It was also assumed that 50% of the CO_2 released by the process arises from calcination of limestone and 50% from the combustion of fuel. Thus, the atmospheric composition input to calculation per gram raw meal is calculated as follows: 0.01g O_2, 0.98 g N_2, 0.22 g CO_2, and 0.18 g H_2O. The clinker solid phases at equilibrium for the temperature range 500 – 1338 °C are presented in Fig. 1. The simulations are truncated at the expected solidus, 1338 °C [43]. Mass loss in Fig. 1 is due to mass transfer from solid to gas phase thus, explaining the disappearance of the alkali at the higher temperatures. Equilibrium calculations were performed at intervals of 2°C and this generates a stepped appearance. In reality, these transitions are smooth owing to kinetic effects. Due to the lack of kinetics/dynamics in the model, real transitions will often depart from predictions based on equilibrium.

Actual observations in modern kilns are complicated by the two stages used; decarbonisation reactions are essentially complete in the suspension preheater and subsequently, the reaction is finished in the rotary kiln where sampling points are limited. The sequence of observed phase changes is shown in Fig. 2, which is an often-reproduced textbook diagram [35] and relates to older single stage operation. While still broadly applicable to modern practice, important differences may occur with the suspension preheater operating at different CO_2 partial pressures than the kiln.

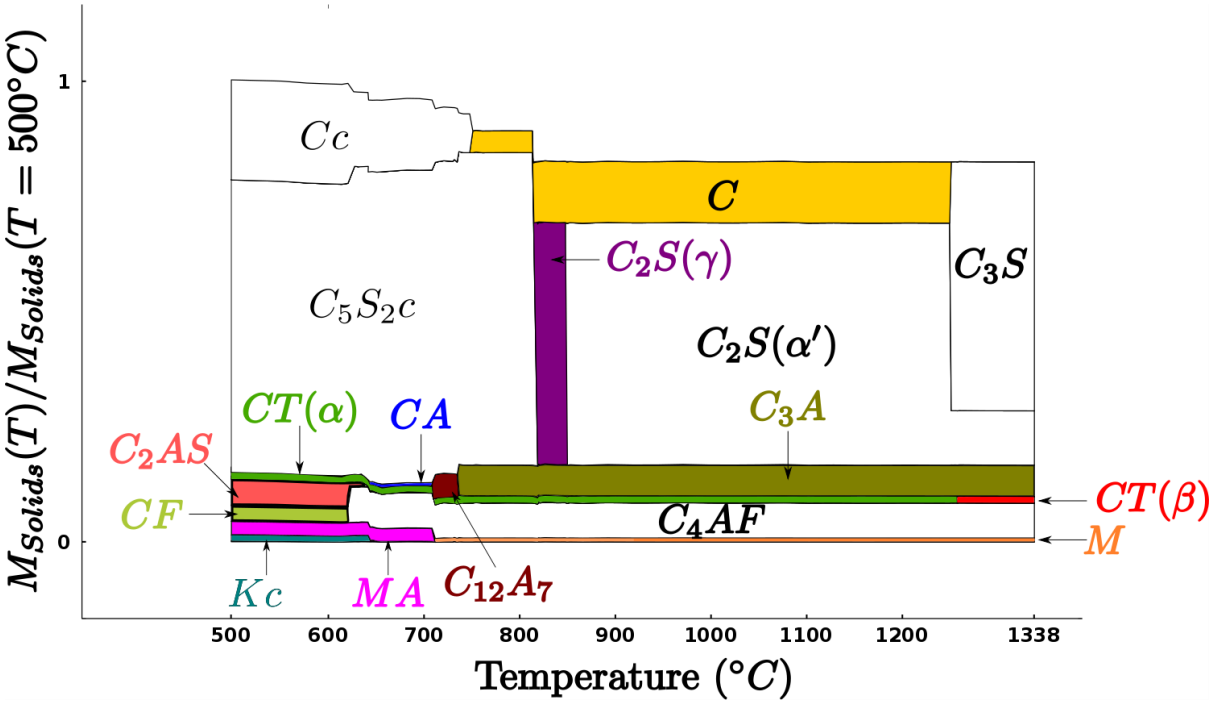

Figure 1: The equilibrium cumulative mass distribution of the solid and liquid phases (relative to the total mass at T = 500 °C) calculated for PC clinker production over the temperature range 500 – 1338 °C. Observed mass loss is due to mass transfer to the gas phase at calculated equilibrium.

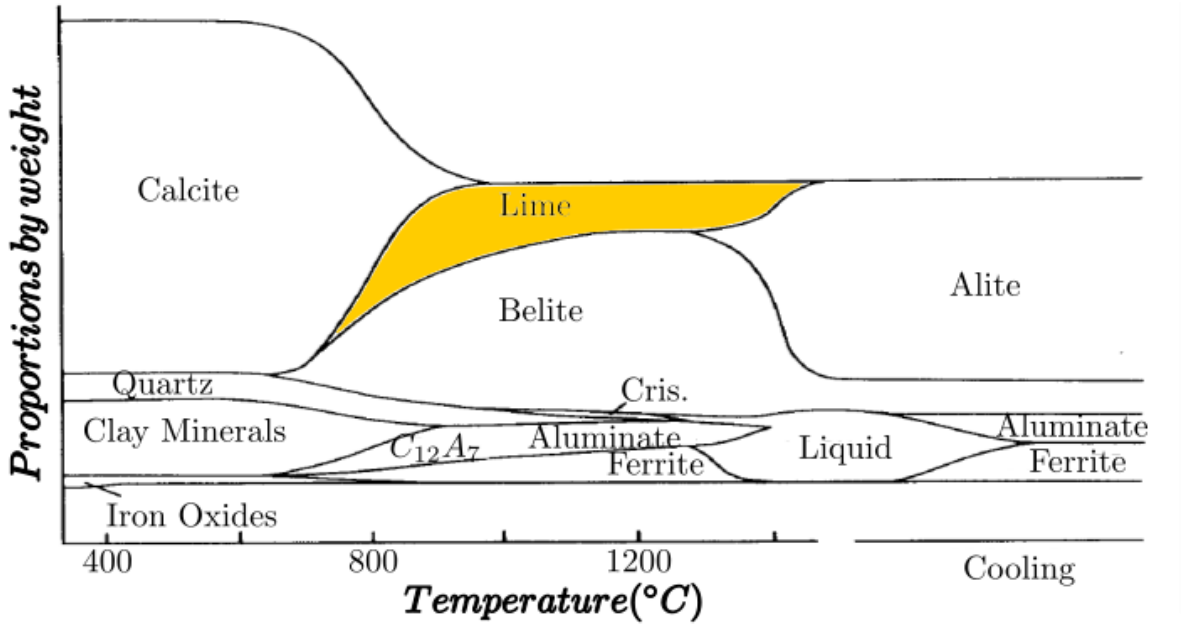

Figure 2: Qualitative representation of expected phase variations during PC clinkering. Adapted from Ref. [35].

If we contrast the practical observation with equilibrium, spurrite (C_5S_2c) is predicted but does not appear except in small quantities and its occurrence is often confined to slow moving meal adhering to the kiln walls or forming rings in single-stage kilns [59-62]. Thus, the equilibrium model developed here reproduces only in part the qualitative phase chemistry with deviations especially apparent at lower temperatures, <1000 °C. If radical changes in clinkering are made, as for example if fluidised bed combustion were used, the course of mineral formation during clinkering could change radically from that of the "observed" model, Fig 2.

Zhang et al. [63] report the experimentally calculated heat of formation from the elements at 298.15 K of spurrite to be -5845.5 ± 10.9 kJ/mol (oxide melt solution calorimetry); this is in agreement with the value calculated (-5847.08 kJ/mol) from the Holland and Powell database [21] and used for calculations in the title study . Also, the entropy of spurrite at 298.15K and 1 bar reported by Holland and Powell (332.0 $kJmol^{-1}K^{-1}$) agrees with that reported by Robie and Hemingway [23] (331.0 $kJmol^{-1}K^{-1}$).

The decomposition temperature of spurrite is reported to be between 750 – 917 °C depending on CO_2 partial pressure [59, 61] and the literature experimental observations are in accord with the decomposition temperatures shown in Fig 3. Bolio-Arceo and Glasser [59] observed the formation of spurrite at 900 °C in a tube furnace with a CO_2 partial pressure of 0.89–0.95 atm; this is also in agreement with calculated spurrite stability. Spurrite decomposition temperature measurements by Glasser [60] give temperatures of spurrite to be 790 ±5 °C and 912 ± 5 °C at CO_2 partial pressures of 0.08 atm and 1 atm respectively; these values are in near agreement although slightly lower than those of the title study at 805 °C and 945 °C respectively.

The remarkable thermal stability of spurrite contrasted with its apparent failure to appear in normal clinkering, have led to additional calculations of its stability; results are shown in Fig 3. Temperature and CO_2 partial pressure are the key variables. Fig. 3 shows only the composition of the individual solid phases with the result that the bulk composition is not constant. The slope of the boundary curves show how progressive decarbonisation occurs as temperature and CO_2 pressure change.

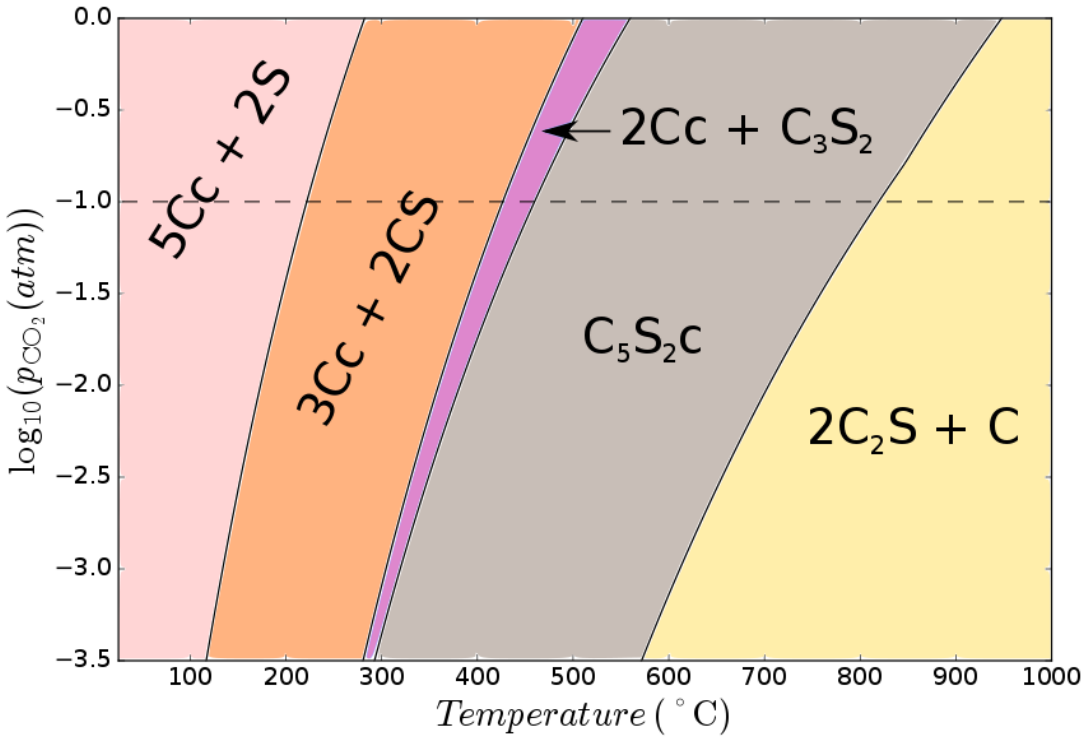

Figure 3: Spurrite stability between 30 - 1000° C as a function of partial pressure of CO_2.The grey broken line denotes where the CO_2 partial pressure is 0.1 atm (~10% by volume); the CO_2 pressure during cement manufacture is usually above this line.

During cement manufacture, incoming air and raw materials have a low CO_2 partial pressure but in zones where calcium carbonate decomposition occurs, and in contact with combustion gas from fossil fuels, the CO_2 pressure rises. Combustion atmospheres nominally have ≈ 4 – 13% CO_2 (depending on fuel) but, decomposition of calcium carbonate in the suspension heater may

increase CO_2 concentrations locally to ≈40%. The grey broken line in Fig. 3 shows the conventional CO_2 pressure in the kiln (10%v or 0.1 atm); the CO_2 pressure is normally at or above this isobar. The curvature of the field boundaries shows the upper temperature limit of stability of spurrite which is enhanced in CO_2-rich atmospheres as may occur in as oxyfuel combustion [64, 65] which typically generate atmospheres rich in CO_2.

4.3 The CaO-Al_2O_3-SiO_2 at subsolidus temperatures

Data for some important phases in the CaO-Al_2O_3-SiO_2 system are yet to be validated. The model of the title study has been used to reproduce the isothermal phase diagrams [35, 66] for the C-A-S system up to 1250 °C. The calculated phase compatibility of the C-A-S system is temperature dependent. Fig. 4 shows how the calculations for the interval: 1000 °C – 1100 °C (left) difers from the calculation for 1150 °C - 1250 °C (right). These diagrams are largely in agreement with the literature [35, 66] except for some minor discrepancies (see red lines in Fig. 4). However, Sahu and Majling [66] report the phase compatibility agrees with Fig. 4 (left) for the temperature range 1000 – 1200 °C. Another discrepancy is with the experimental results observed in Ref. [15] where the phase compatibility at 1250 °C agrees with Fig. 4 (left) rather than Fig. 4 (right) for 1250°C. It is of course possible that some substitution occurs in the relevant solids and influences the observed coexistences but the free energy difference between phases approaches zero so any error in the numerical values of the free energy will strongly influence the calculation. It is clear that better data are needed.

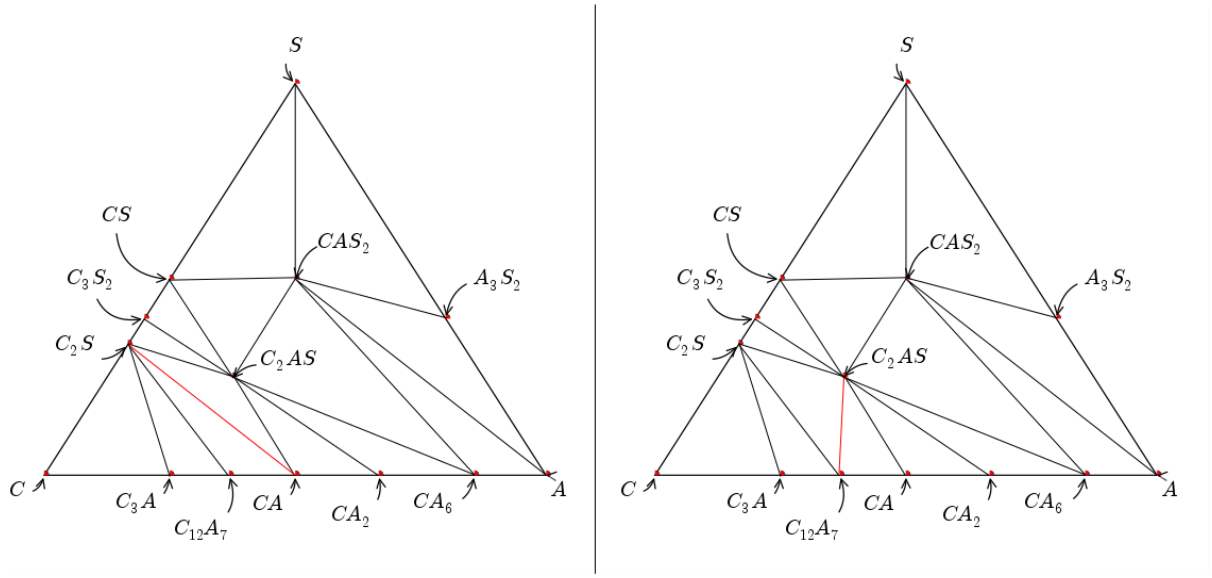

Figure 4: Ternary phase diagrams (mole) of the C-A-S system produced from the database compiled in the title paper. The diagram on the left is produced at temperatures of 1000° C, 1050° C, and 1100° C. The diagram on the right is produced at temperatures of 1150 °C, 1200 °C, and 1250 °C. Above 1250 °C, alite (C_3S) is stabilised.

5 Discussion and future work

An improved database for calculation of thermodynamic functions of cement systems is presented and application examples are given. Nevertheless, some knowledge gaps remain, and predictions made from thermodynamic model may need experimental verification before being accepted; however, calculation certainly reduces the amount of experimental work needed. The next steps are to extend the database and to deal with solid solution formation as well as melting and freezing processes; this will include the dependence of the Al/Fe ratio in the ferrite phase on temperature. These tasks are not trivial, models often need approximations when dealing with solution phases, solid or liquid, and in its present state, the database will not predict element fractionation between phases or the existence of metastable transitions such as formation of beta belite during cooling.

The developed model does include the process atmosphere and enable calculation of gas-solid reactions; the calculation of spurrite stability is an example of how. The development of novel cements, such as calcium sulfoaluminates can be driven by thermodynamic calculations showing, for example, conditions under which ye'elimite is stable [67]. The feasibility of making calcium sulfoaluminate was piloted by thermodynamic calculation before trials were made [7, 9, 68]. Likewise the conditions for ternesite formation were delineated by calculation [8]. Additionally, the database/model has been used to predict compatibility regions for formation of alite-calcium sulfoaluminate clinkers [14]. Thermodynamic data for ye'elimite and ternesite are not included in the compilation of the title study as they are still being developed; however, current available data can be found in Refs. [8, 67, 69-71].

Future work will also need to focus on thermodynamic data relevant to assessing the role of minor components such as Mg, Ti, F, Cl, Zn, P, Na, K, Sr, and Br which will affect relative free energies and stabilities; for example, as shown by the mineralisation, stabilisation, and lower formation temperature of alite [72].

6 Conclusion

A high-temperature thermodynamic dataset for cement clinkering equilibrium calculations is reviewed, compiled, and presented; the dataset is also validated through a series of case studies. The dataset and model can be used to calculate heat balances and conduct limited predictive modelling. The information presented here is beneficial to develop novel cement formulations and production processes; equally, it will find use by cement producers looking to optimise production and for quality control.

The data is provided in electronic format as downloadable supplementary material with this article (S1, S2, and S3). This database will be updated over time, but this study can serve as a benchmark of thermodynamic data for cement clinkering.

8 Additional information

This work began as part of a PhD project; further information related to the development of this dataset can be found in the published thesis available online [73]. The database presented here is the initial cement thermodynamic data parsed in SimCem along with other thermodynamic data which can be found at www.SimCem.com.

9 Acknowledgements

This work was supported, in part, by the Engineering and Physical Science Research Council (EPSRC) through grant: EP/R025959/1.

7 References

1. Olivier, J.G.J., et al., *Trends in global CO2 emissions: 2016 Report*. 2016, PBL Netherlands Environmental Assessment Agency Hague and European Commission Joint Research Centre Institute for Environment and Sustainability.
2. Andrew, R.M., *Global CO 2 emissions from cement production.* Earth System Science Data, 2018. **10**(1): p. 195.
3. Gartner, E. and H. Hirao, *A review of alternative approaches to the reduction of CO 2 emissions associated with the manufacture of the binder phase in concrete.* Cement and Concrete research, 2015. **78**: p. 126-142.
4. Isteri, V., et al., *Production and properties of ferrite-rich CSAB cement from metallurgical industry residues.* Science of The Total Environment, 2019: p. 136208.
5. Hanein, T., J.-L. Galvez-Martos, and M.N. Bannerman, *Carbon footprint of calcium sulfoaluminate clinker production.* Journal of Cleaner Production, 2018. **172**: p. 2278-2287.
6. Bogue, R.H., *Calculation of the compounds in Portland cement.* Industrial & Engineering Chemistry Analytical Edition, 1929. **1**(4): p. 192-197.
7. Hanein, T., et al., *Production of belite calcium sulfoaluminate cement using sulfur as a fuel and as a source of clinker sulfur trioxide: pilot kiln trial.* Advances in Cement Research, 2016. **28**(10): p. 643-653.

8. Hanein, T., et al., *Stability of ternesite and the production at scale of ternesite-based clinkers.* Cement and Concrete Research, 2017. **98**(C): p. 91-100
9. Bannerman, M.N., T. Hanein, and F.P. Glasser, *Validation of a one-dimensional kiln heat transfer model against a pilot kiln*, in *37th Cement ad Concrete Science Conference*. 2017: London.
10. Le Chatelier, H., *Experimental researches on the constitution of hydraulic mortars*. 1905: McGraw Publishing Company.
11. Davies, R.H., et al., *MTDATA - thermodynamic and phase equilibrium software from the national physical laboratory.* Calphad, 2002. **26**(2): p. 229-271.
12. Bale, C.W., et al., *FactSage thermochemical software and databases.* Calphad, 2002. **26**(2): p. 189-228.
13. Hanein, T., F.P. Glasser, and M. Bannerman. *Thermodynamics of Portland Cement Clinkering.* in *14th International Congress on the Chemistry of Cement.* 2015. Beijing, China.
14. Hanein, T., et al., *Alite calcium sulfoaluminate cement: chemistry and thermodynamics.* Advances in Cement Research, 2019. **31**(3): p. 94-105.
15. Galan, I., et al., *Phase Compatibility in the System CaO–SiO2–Al2O3–SO3–Fe2O3 and the Effect of Partial Pressure on the Phase Stability.* Industrial & Engineering Chemistry Research, 2017. **56**(9): p. 2341-2349.
16. Galan, I., et al., *Advances in clinkering technology of calcium sulfoaluminate cement.* Advances in Cement Research, 2017.
17. McBride, B.J., M.J. Zehe, and S. Gordon, *NASA Glenn coefficients for calculating thermodynamic properties of individual species*. 2002: National Aeronautics and Space Administration, John H. Glenn Research Center at Lewis Field.
18. Smith, G.P., et al. *GRI-Mech 3.0:* http://www.me.berkeley.edu/gri_mech/. http://combustion.berkeley.edu/gri-mech/ [cited 2019.
19. Babushkin, V.I., G.M. Matveev, and O.P. McHedlov-Petrosian, *Thermodynamics of silicates*. 1985: Springer-Verlag Berlin.
20. Haas Jr, J.L., G.R. Robinson Jr, and B.S. Hemingway, *Thermodynamic tabulations for selected phases in the system CaO-Al2O3-SiO2-H2 at 101.325 kPa (1 atm) between 273.15 and 1800 K.* Journal of Physical and Chemical Reference Data, 1981. **10**(3): p. 575-670.
21. Holland, T.J.B. and R. Powell, *An improved and extended internally consistent thermodynamic dataset for phases of petrological interest, involving a new equation of state for solids.* Journal of Metamorphic Geology, 2011. **29**(3): p. 333-383.
22. Barin, I., et al., *Thermochemical data of pure substances*. Vol. 6940. 1993: VCH Weinheim.
23. Robie, R.A. and B.S. Hemingway, *Thermodynamic properties of minerals and related substances at 298.15 K and 1 bar (10^5 pascals) pressure and at higher temperatures.* 1995.
24. Berman, R.G., *Internally-consistent thermodynamic data for minerals in the system Na2O-K2O-CaO-MgO-FeO-Fe2O3-Al2O3-SiO2-TiO2-H2O-CO2.* Journal of petrology, 1988. **29**(2): p. 445-522.
25. Wagman, D.D., et al., *The NBS tables of chemical thermodynamic properties. Selected values for inorganic and C1 and C2 organic substances in SI units*. 1982, DTIC Document.
26. Kelley, K.K., *High-temperature heat-content, heat-capacity, and entropy data for the elements and inorganic compounds.* US Bureau of Mines Bull., 1960. **584**: p. 232.
27. Bard, A.J., R. Parsons, and J. Jordan, *Standard potentials in aqueous solution*. Vol. 6. 1985: CRC press.
28. Bonnickson, K.R., *High temperature heat contents of aluminates of calcium and magnesium.* The Journal of Physical Chemistry, 1955. **59**(3): p. 220-221.
29. Lothenbach, B., et al., *Thermodynamic modelling of the effect of temperature on the hydration and porosity of Portland cement.* Cement and Concrete Research, 2008. **38**(1): p. 1-18.

30. Herfort, D., *Chemistry of the Clinker Production Process.* KUEI SUAN JEN HSUEH PAO, 2015. **43**(10): p. 1314-1323.
31. Coughlin, J.P., *Heats of formation of crystalline CaO· Al2O3, 12CaO· 7Al2O3, and 3CaO· Al2O3.* Journal of the American Chemical Society, 1956. **78**(21): p. 5479-5482.
32. Huber Jr, E.J. and C.E. Holley Jr, *The heat of combustion of calcium.* The Journal of Physical Chemistry, 1956. **60**(4): p. 498-499.
33. Geiger, C.A., et al., *Enthalpies of formation of CaAl 4 O 7 and CaAl 12 O 19 (hibonite) by high temperature, alkali borate solution calorimetry.* Geochimica et Cosmochimica Acta, 1988. **52**(6): p. 1729-1736.
34. Petaev, M.I. *Revised Thermodynamic Properties of Ca Aluminates: Implications for the Condensation Sequences*.
35. Taylor, H.F.W., *Cement chemistry.* Telford, London, 1997.
36. Hillert, M., et al., *A reevaluation op the rankinite phase in the CaO-SiO 2 system.* Calphad, 1991. **15**(1): p. 53-58.
37. Holland, T.J.B. and R. Powell, *An internally consistent thermodynamic data set for phases of petrological interest.* Journal of metamorphic Geology, 1998. **16**(3): p. 309-343.
38. Thorvaldson, T., R.R. Edwards, and E.C. Bailey, *Die Bildungswärme von Tetracalciumaluminiumferrit.* Zeitschrift für anorganische und allgemeine Chemie, 1938. **236**(1): p. 310-319.
39. Zhu, Z., et al., *Thermodynamics of Reactions Among Al2O3, CaO, SiO2 and Fe2O3 During Roasting Processes.* 2011.
40. Bonnickson, K.R., *High temperature heat contents of calcium and magnesium ferrites.* Journal of the American Chemical Society, 1954. **76**(6): p. 1480-1482.
41. Newman, E.S. and R. Hoffman, *Heats of Formation of Hexacalcium Dialumino Ferrite and Dicalcium Ferrite.* Journal of Research of the National Bureau of Standards, 1956. **56**(6): p. 313.
42. Newman, E.S., *Heats of Solution of Solid Solutions of Hexacalcium Dialumino Ferrite and Dicalcium Ferrite.* JOURNAL OF RESEARCH OF THE NATIONAL BUREAU OF STANDARDS, 1947. **38**(6): p. 661-664.
43. Glasser, F.P., et al., *Advances in cement clinkering.* Inovations in Portland Cement Manufacture, 2004. **332**.
44. Pliego-Cuervo, Y.B. and F.P. Glasser, *Role of sulphates in cement clinkering: The calcium silicosulphate phase.* Cement and Concrete Research, 1978. **8**(4): p. 455-459.
45. Meija, J., et al., *Isotopic compositions of the elements 2013 (IUPAC technical Report).* Pure and Applied Chemistry, 2016. **88**(3): p. 293-306.
46. Audi, G., et al., *The Ame2012 atomic mass evaluation.* Chinese physics C, 2012. **36**(12): p. 1287.
47. Wang, M., et al., *The Ame2012 atomic mass evaluation.* Chinese Physics C, 2012. **36**(12): p. 1603.
48. Waldbaum, D.R., *Thermodynamic properties of mullite, andalusite, kyanite and sillimanite.* Am Mineral, 1965. **50**: p. 186-195.
49. King, E.G., D.R. Torgeson, and O.A. Cook, *High-Temperature Heat Contents of 3CaO· B2O3, 2CaO· B2O3, CaO· B2O3, and CaO· 2B2O31.* Journal of the American Chemical Society, 1948. **70**(6): p. 2160-2163.
50. Naylor, B.F. and O.A. Cook, *High-Temperature Heat Contents of the Metatitanates of Calcium, Iron and Magnesium1.* Journal of the American Chemical Society, 1946. **68**(6): p. 1003-1005.
51. King, E.G., R.L. Orr, and K.R. Bonnickson, *Low temperature heat capacity, entropy at 298.16 K., and high temperature heat content of sphene (CaTiSiO5).* Journal of the American Chemical Society, 1954. **76**(17): p. 4320-4321.

52. Orr, R.L., *High temperature heat contents of magnesium orthosilicate and ferrous orthosilicate.* Journal of the American Chemical Society, 1953. **75**(3): p. 528-529.
53. Shomate, C.H., *Heat Capacities at Low Temperatures of the Metatitanates of Iron, Calcium and Magnesium1.* Journal of the American Chemical Society, 1946. **68**(6): p. 964-966.
54. Orr, R.L. and J.P. Coughlin, *High temperature heat contents of magnesium orthotitanate and magnesium dititanate.* Journal of the American Chemical Society, 1952. **74**(12): p. 3186-3187.
55. Naylor, B.F., *High-Temperature Heat Contents of Na2TiO3, Na2Ti2O5 and Na2Ti3O71.* Journal of the American Chemical Society, 1945. **67**(12): p. 2120-2122.
56. Kawajir, Y., C. Laird, and A. Waechter, *Introduction to IPOPT: a tutorial for downloading, installing, and using IPOPT (2015).* URL: http://www. coinor. org/Ipopt/documentation.
57. Hökfors, B., et al., *On the phase chemistry of Portland cement clinker.* 2014.
58. Campbell, D.H., *Microscopical examination and interpretation of portland cement and clinker*. 1986: Construction Technology Laboratories.
59. Bolio-Arceo, H. and F.P. Glasser, *Formation of spurrite, Ca5(SiO4)2CO3.* Cement and Concrete Research, 1990. **20**(2): p. 301-307.
60. Glasser, F.P., *The formation and thermal stability of spurrite, Ca5(SiO4)2CO3.* Cement and Concrete Research, 1973. **3**(1): p. 23-28.
61. Goswami, G., B.P. Padhy, and J.D. Panda, *Thermal analysis of spurrite from a rotary cement kiln.* Journal of Thermal Analysis and Calorimetry, 1989. **35**(4): p. 1129-1136.
62. Kurdowski, W. and M. Soboń, *Mineral composition of build-up in cement kiln preheater.* Journal of Thermal Analysis and Calorimetry, 1999. **55**(3): p. 1021-1029.
63. Zhang, Y.-Q., A.V. Radha, and A. Navrotsky, *Thermochemistry of two calcium silicate carbonate minerals: scawtite, Ca7 (Si6O18)(CO3)· 2H2O, and spurrite, Ca5 (SiO4) 2 (CO3).* Geochimica et Cosmochimica Acta, 2013. **115**: p. 92-99.
64. Hökfors, B., E. Viggh, and M. Eriksson, *Simulation of oxy-fuel combustion in cement clinker manufacturing.* Advances in Cement Research, 2015. **27**(1): p. 42-49.
65. Eriksson, M., B. Hökfors, and R. Backman, *Oxyfuel combustion in rotary kiln lime production.* Energy Science & Engineering, 2014. **2**(4): p. 204-215.
66. Sahu, S. and J. Majling, *Phase compatibility in the system CaO・SiO2・Al2O3・Fe2O3・SO3 referred to sulphoaluminate belite cement clinker.* Cement and Concrete Research, 1993. **23**(6): p. 1331-1339.
67. Hanein, T., et al. *Thermodynamic data of ye'elemite (C4A3S) for cement clinker equilibrium calculations*. in *35th Cement & Concrete Science Conference.* 2015. Aberdeen.
68. Hanein, T., et al. *Optimising calcium sulfoaluminate cements*.
69. Costa, U., F. Massazza, and M. Testolin, *Heats of formation of C4A3S, 4SrOÁ3Al2O3.* Il Cemento, 1972. **2**: p. 61-8.
70. Skalamprinos, S., et al., *Enthalpy of formation of ye'elimite and ternesite.* Journal of thermal analysis and calorimetry, 2018. **131**(3): p. 2345-2359.
71. Pisch, A. and A. Pasturel, *On the heat of formation of ye'elimite Ca4Al6O12. SO4 using density functional theory.* Advances in Cement Research, 2018. **31**(3): p. 106-112.
72. Shame, E.G. and F.P. Glasser, *Stable Ca 3 SiO 5 solid solutions containing fluorine and aluminium made between 1050 and 1250 C.* BR. CERAM. TRANS. J. Br. Ceram. Trans. J., 1987. **86**(1): p. 13.
73. Hanein, T., *Development of a novel calcium sulfoaluminate cement production process, PhD thesis*, in *School of Engineering & School of Natural and Computing Sciences*. 2016, University of Aberdeen.